Inorganic Chemistry

Article

pubs.acs.org/IC

Hydrothermal Derived LaOF:Ln^{3+} (Ln = Eu, Tb, Sm, Dy, Tm, and/or Ho) Nanocrystals with Multicolor-Tunable Emission Properties

Mengmeng Shang,[†,‡] Dongling Geng,[†,‡] Xiaojiao Kang,[†,‡] Dongmei Yang,[†,‡] Yang Zhang,[†,‡] and Jun Lin*[,†]

[†]State Key Laboratory of Rare Earth Resource Utilization, Changchun Institute of Applied Chemistry, Chinese Academy of Sciences, Changchun 130022, P. R. China

[‡]University of Chinese Academy of Sciences, Beijing 100049, P. R. China

Supporting Information

ABSTRACT: A series of LaOF:Ln^{3+} (Ln = Eu, Tb, Sm, Dy, Tm, and/or Ho) nanocrystals with good dispersion have been successfully prepared by the hydrothermal method followed a heat-treatment process. Under ultraviolet radiation and low-voltage electron beam excitation, the LaOF:Ln^{3+} nanocrystals show the characteristic f-f emissions of Ln^{3+} (Ln = Eu, Tb, Sm, Dy, Tm, or Ho) and give red, blue-green, orange, yellow, blue, and green emission, respectively. Moreover, there exists simultaneous luminescence of Tb^{3+}, Eu^{3+}, Sm^{3+}, Dy^{3+}, Tm^{3+}, or Ho^{3+} individually when codoping them in the single-phase LaOF host (for example, LaOF:Tb^{3+}, Eu^{3+}/Sm^{3+}; LaOF:Tm^{3+}, Dy^{3+}/Ho^{3+}; LaOF:Tm^{3+}, Ho^{3+}, Eu^{3+} systems), which is beneficial to tune the emission colors. Under low-voltage electron beam excitation, a variety of colors can be efficiently adjusted by varying the doping ions and the doping concentration, making these materials have potential applications in field-emission display devices. More importantly, the energy transfer from Tm^{3+} to Ho^{3+} in the LaOF:Tm^{3+}, Ho^{3+} samples under UV excitation was first investigated and has been demonstrated to be a resonant type via a quadrupole-quadrupole mechanism. The critical distance (R_{Tm-Ho}) is calculated to be 28.4 Å. In addition, the LaOF:Tb^{3+} and LaOF:Tm^{3+} phosphors exhibit green and blue luminescence with better chromaticity coordinates, color purity, and higher intensity compared with the commercial green phosphor ZnO:Zn and blue phosphor Y_2SiO_5:Ce^{3+} to some extent under low-voltage electron beam excitation.

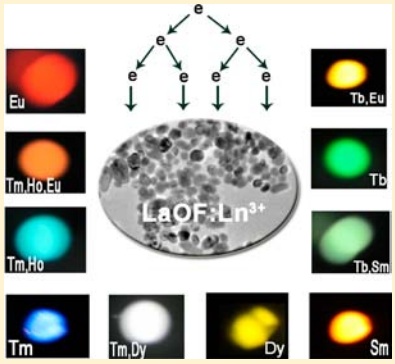

1. INTRODUCTION

As the hot spot in display areas, field emission displays (FEDs) have gained a great interest and been considered as one of the most promising technologies in the flat panel display market due to their attractive features such as thin panels, self-emission, wide viewing, quick response time, high brightness, high contrast ratio, lightweight, and low power consumption.[1−4] Phosphors are efficient luminescence materials and irreplaceable components for the development of FEDs. Recently, oxide phosphors for FEDs have gained interest due to their better thermal and chemical stability and environmental friendliness compared with sulfides, which are currently used in the screen of FEDs.[5−10] Moreover, rare-earth doped, oxide-based phosphors for FEDs have been of great interest due to their excellent light output, color-rendering properties, and superior stability under electron bombardment.[11−13] On the other hand, since the scattering efficiency of a particle depends on the diameter of the particle,[14] using nanosized luminescent material is an appropriate strategy for suppressing the scattering loss.[15] In addition, particles whose diameter is smaller than 50 nm can be transparently dispersed in a matrix, showing the negligible scattering of visible light.[16] Therefore, reducing the particle size to the nanometer scale would essentially eliminate the backscattering loss in the FEDs. Furthermore, the nanosized luminescent materials are propitious to produce a compact phosphor screen and thus to improve its CL properties.

Lanthanum oxyfluoride, LaOF, has been investigated widely in many fields due to the advantages of favorable thermal and chemical stability.[17,18] Since the La^{3+} ion has the largest ionic radius among the lanthanide series of ions, it can be easily substituted by different Ln^{3+} ions in the structure. However, the majority of research on LaOF has been done on their bulk crystals obtained by annealing of LaF_3 in air atmosphere or using solid state reactions between La_2O_3 and LaF_3 (or NH_4F).[18−20] Recently, we have successfully synthesized nanosized LaOF:Eu^{3+} phosphor with good dispersion by a mild condition via a facile hydrothermal method followed by a heat treatment and realized the white and color-tuning emission properties in the LaOF:Eu^{3+} system.[21] As a continuation and extension of this work, here we report the synthesis of LaOF:Ln^{3+} (Ln = Eu, Tb, Sm, Dy, Tm, and/or Ho) nanocrystals and investigate their PL and CL properties in more detail. There exists energy transfer between Ln^{3+} ions and multicolor emissions in the co- or tridoped LaOF systems. The corresponding luminescence mechanisms have been discussed in detail.

Received: July 29, 2012
Published: September 28, 2012

2. EXPERIMENTAL SECTION

2.1. Chemicals and Materials. The rare-earth oxides, including La_2O_3, Eu_2O_3, Tb_4O_7, Sm_2O_3, Dy_2O_3, Tm_2O_3, and Ho_2O_3 (all with purity of 99.999%), were purchased from Science and Technology Parent Company of Changchun Institute of Applied Chemistry. A colorless stock solution of $Ln(NO_3)_3$ (Ln = La, Eu, Tb, Sm, Dy, Tm, Ho) with a certain concentration was prepared by dissolving its corresponding rare-earth oxides in dilute HNO_3. Other chemicals were purchased from the Beijing Chemical Company. All chemicals were of analytical grade reagents and used directly without further purification.

2.2. Preparation of $LaCO_3F$:*x* mol % Ln^{3+} (*x* = 0−15, Ln = Eu, Tb, Sm, Dy, Tm, and/or Ho) Precursors. In a typical procedure of preparing representative $LaCO_3F$:5 mol % Eu^{3+} nanocrystals, 1.95 mmol $La(NO_3)_3$, 0.05 mmol $Eu(NO_3)_3$, and 4 mmol trisodium citrate (labeled as Cit^{3-}, the molar ratio of Cit^{3-}:La^{3+} is 2:1) were dissolved in deionized water to form 40 mL of solution, and then a certain amount of NaF and Na_2CO_3 was added into the above solution. After vigorously stirring for 30 min (the pH of the solution is 9), the obtained mixture was transferred into a Teflon bottle (50 mL), held in a stainless steel autoclave, sealed, and maintained at 180 °C for 24 h. As the autoclave cooled to room temperature naturally, the precipitate was separated by centrifugation and washed with deionized water and ethanol in sequence. Finally, the precipitate was dried in air at 80 °C for 12 h.

2.3. Preparation of Nonaggregated LaOF:*x* mol % Ln^{3+} Nanocrystals. The as-prepared $LaCO_3F$:*x* mol % Ln^{3+} precursor was dispersed in the anhydrous alcohol. A few drops of oleic acid were added into the above suspension and ultrasonically treated for 20 min to make oleic acid coat on the surface of $LaCO_3F$:Ln^{3+} nanoparticles entirely. At last the particles were separated by centrifugation and dried in air at 60 °C. The final LaOF:Ln^{3+} products were retrieved through a heat treatment of the $LaCO_3F$:Ln^{3+} precursors at 600 °C in air for 4 h with a heating rate of 1 °C/min.

Characterization. Power X-ray diffraction (XRD) measurements were performed on a D8 Focus diffractometer at a scanning rate of 10°/min in the 2θ range from 20° to 80°, with graphite monochromatized Cu Kα radiation (λ = 0.15405 nm). The composition of the samples was inspected using a field-emission scanning electron microscope (FE-SEM, S-4800, Hitachi) equipped with an energy-dispersive X-ray (EDX) spectrometer. Transmission electronmicroscopy (TEM) were recorded using a FEI Tecnai G2S-Twin with a field-emission gun operating at 200 kV. Images were acquired digitally on a Gatan multipole CCD camera. Photoluminescence (PL) excitation and emission spectra were recorded with a Hitachi F-7000 spectrophotometer equipped with a 150 W xenon lamp as the excitation source. Cathodoluminescence (CL) measurements were carried out in an ultrahigh-vacuum chamber ($<10^{-8}$ Torr), where the phosphors were excited by an electron beam in the voltage range of 2.0−7.0 kV and different filament currents, and the emission spectra were recorded using an F-7000 spectrophotometer. All of the measurements were performed at room temperature.

3. RESULTS AND DISCUSSION

3.1. Phase Identification and Morphology. The composition and phase purity of the products were first examined by XRD and EDX. Figure 1A shows the XRD patterns of the as hydrothermally synthesized and annealed products. On the basis of the Joint Committee on Power Diffraction Standard (JCPDS) reference database, the diffraction peaks of the as-synthesized precursor sample (curve a in Figure 1A) can be assigned to a pure hexagonal $LaCO_3F$ phase, which coincides well with the literature values (JCPDS no. 41-0595). No peak shifts and other impurity phases appear in this figure, indicating the high purity and crystallinity of the product. The crystallite size of the studied samples can be estimated from the Scherrer equation, $D = 0.941\lambda/\beta\cos\theta$, where D is the average grain size, the factor 0.941 is characteristic of

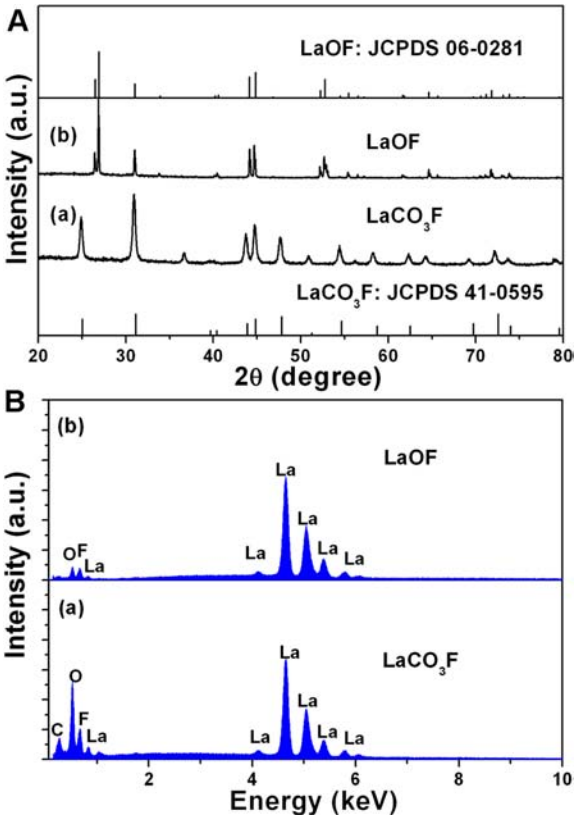

Figure 1. (A) The XRD patterns of (a) as-prepared $LaCO_3F$ precursor and (b) LaOF obtained by calcining the $LaCO_3F$ precursor at 600 °C for 4 h. The standard data of hexagonal $LaCO_3F$ (JCPDS no. 41-0595) and rhombohedral LaOF (JCPDS no. 06-0281) are shown as references. (B) EDX spectra of (a) as-prepared $LaCO_3F$ and (b) LaOF obtained by calcining $LaCO_3F$ at 600 °C in air for 4 h.

spherical objects, λ is the X-ray wavelength (0.15405 nm), and θ and β are the diffraction angle and full-width at half-maximum (fwhm, in radian) of an observed peak, respectively.[22] The estimated average crystallite size is about 30 nm. The product obtained by calcination of the $LaCO_3F$ precursor at 600 °C for 4 h crystallizes in the trigonal γ-phase of LaOF (JCPDS no. 06-0281), as shown in curve b (Figure 1A). So, the LaOF samples were obtained by calcining $LaCO_3F$ through releasing CO_2. Figure 1B shows the energy-dispersive X-ray (EDX) spectra of the as-prepared $LaCO_3F$ precursor and the LaOF sample. The EDX spectra further confirm the presence of La, C, O, and F from the precursor sample (spectrum a in Figure 1B). After calcination at 600 °C for 4 h, the element C disappeared, and the sample only consists of La, O, and F (spectrum b in Figure 1B). This result is consistent with that of XRD. Due to the similar ion radius and chemical property, doping a certain amount of Ln^{3+} (Ln = Eu, Tb, Sm, Dy, Tm, and/or Ho) ions would not have a great influence on the formation of the products. This inference can be evidenced by the XRD patterns of a variety of Ln^{3+} ions doped samples. Figure S1 (Supporting Information) and Figure 2 show the XRD patterns of the different activators doped precursors and annealed products, respectively. It is obviously seen that all the diffraction peaks of those samples coincide with the pure hexagonal phase of $LaCO_3F$ and trigonal γ-phase of LaOF according to the patterns shown in Figure 1A. No other phase or impurity can be detected, indicating that Ln^{3+} (Ln = Eu, Tb, Sm, Dy, Tm,

dx.doi.org/10.1021/ic301662c | Inorg. Chem. 2012, 51, 11106−11116

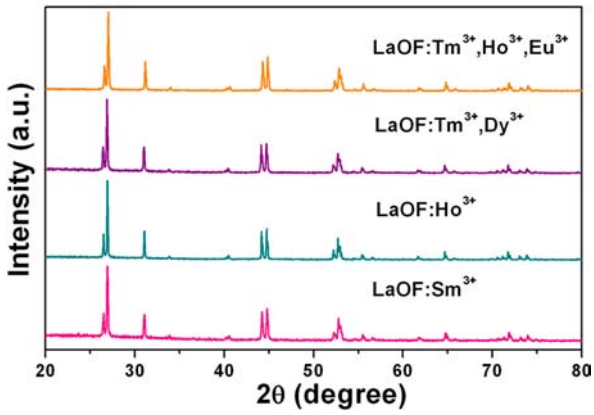

Figure 2. The representative XRD patterns of the LaOF:Sm^{3+}, LaOF:Ho^{3+}, LaOF:Sm^{3+}, LaOF:Tm^{3+}, Dy^{3+}, and LaOF:Tm^{3+}, Ho^{3+}, Eu^{3+} samples by calcining their precursor at 600 °C for 4 h.

and/or Ho) ions were completely dissolved in the $LaCO_3F$ precursor and the LaOF annealed product.

Using the trisodium citrate assisted hydrothermal method, the products are mainly composed of well-separated round nanoparticles. It should be mentioned that the low amount of doped ions (Ln^{3+}) did not change the phase, crystallization, or morphology of the $LaCO_3F$ and LaOF samples, and all the results are similar with our previous work.[21] So here we only gave the TEM image of the LaOF sample to illustrate briefly. The TEM and HRTEM images of the $LaCO_3F$ and LaOF samples are shown in Figure 3A and B, respectively. It can be

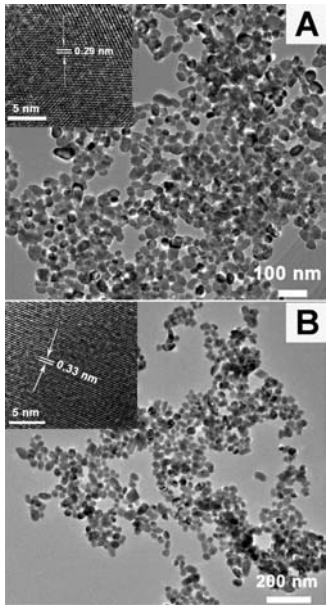

Figure 3. TEM and HRTEM images of the $LaCO_3F$ (A) and LaOF (B) samples.

seen clearly that the as-obtained $LaCO_3F$ sample consists of well-separated nanoparticles with sizes of about 30−50 nm (Figure 3A). The HRTEM image (inset in Figure 3A) shows lattice planes with perfect crystallinity. The lattice fringes show the imaging characteristics of the hexagonal $LaCO_3F$ crystal, in which the *d*-spacing of 0.29 nm corresponds to the lattice distance between the (112) planes. The TEM image of LaOF obtained by heating the $LaCO_3F$ precursor with oleic acid treatment before calcining is shown in Figure 3B. It can be clearly seen that the obtained LaOF sample with oleic acid treatment can still maintain good dispersion. The HRTEM image (inset in Figure 3B) shows lattice planes with perfect crystallinity. The lattice fringes show the imaging characteristics of the rhombohedral LaOF crystal, in which the *d*-spacing of 0.33 nm corresponds to the lattice distance between the (012) planes. All the results are consistent with those of XRD.

3.2. Photoluminescence Properties. The photoluminescence spectra of Ln^{3+} (Ln = Eu, Tb, Sm, Dy, Tm, or Ho) ion doped $LaCO_3F$ precursors are shown in Figure S2 (Supporting Information). It can be observed that the photoluminescence properties of all samples are not very good, which is due to the existence of oxocarbonate anions (CO_3^{2-}) in the precursor $LaCO_3F$ lattice with higher vibrational energy (1439 cm^{-1}) that will cause luminescence quenching. For the Eu^{3+} ion doped $LaCO_3F$ precursor (Figure S2a, Supporting Information), its photoluminescence excitation spectrum monitored at 593 nm consists of a broad band from 200 to 310 nm and some narrow lines beyond 310 nm. The broad excitation band centered at about 273 nm is attributed to the O^{2-}−Eu^{3+} charge transfer band (CTB); upon excitation into the O^{2-}−Eu^{3+} charge transfer band (CTB) at 273 nm, the emission spectrum of the $LaCO_3F$:0.03Eu^{3+} sample is dominated by the orange emission transition $^5D_0 \rightarrow {}^7F_1$ (593 nm) accompanied by the presence of other transitions of the Eu^{3+} ion within its $4f^6$ configuration, which indicates that the Eu^{3+} ions are located at sites with inversion symmetry in the $LaCO_3F$ host lattice. The $LaCO_3F$:0.03Tb^{3+} sample (Figure S2b, Supporting Information) gives weak green emission due to the characteristic $^5D_4 \rightarrow {}^7F_5$ emission of Tb^{3+} ion under the excitation of $4f^8 \rightarrow 4f^7 5d$ absorption band of Tb^{3+}. Moreover, Sm^{3+}, Dy^{3+}, Tm^{3+}, and Ho^{3+} singly doped $LaCO_3F$ precursor samples show their respective characteristic emissions under the excitation of their f-f line absorption, as shown in Figure S2c-f (Supporting Information). Their photoluminescence properties will not be given a detailed description here, and, as a result, the similar photoluminescence properties for the Eu^{3+}, Tb^{3+}, Sm^{3+}, Dy^{3+}, Tm^{3+}, and Ho^{3+} single- or codoped LaOF samples obtained by annealing $LaCO_3F$:Ln^{3+} precursors are discussed in detail in the next.

Figure 4 presents the photoluminescence spectra of Ln^{3+} (Ln = Eu, Tb, Sm, Dy, Tm, or Ho) ion doped LaOF samples. As one of the most frequently used red emitting activators in rare-earth ions doped materials, the Eu^{3+} ion mainly shows characteristic emissions resulting from the transitions of $^5D_{0,\,1,\,2} \rightarrow {}^7F_J$ (J = 0, 1, 2, 3, 4). The LaOF:$x$$Eu^{3+}$ (x = 0.004, 0.05) samples were selected as the representative examples to discuss the PL properties of Eu^{3+} ions in the LaOF host. As shown in Figure 4a, the excitation spectrum monitored with 613 nm consists of broad excitation bands from 200 to 320 nm (two weak broad bands below 250 nm and a strong one with a maximum at 274 nm) and some narrow lines beyond 350 nm. The strong band with a maximum at 274 nm is due to the charge transfer transition between O^{2-} and Eu^{3+}, and the other two weak bands below 250 nm should be ascribed to the host absorption.[21] The narrow lines beyond 350 nm are the characteristic f → f transitions of Eu^{3+} within its $4f^6$ configuration.[23] Excitation into the CTB of Eu^{3+}−O^{2-} at 274 nm yields different emission spectra, as shown by the red line and the blue line in Figure 4a. The emission spectrum of LaOF:0.004Eu^{3+} (blue line) consists of all the emission lines from the $^5D_{0,1,2,3}$ excited states to the ^7F_J ground states of Eu^{3+},

dx.doi.org/10.1021/ic301662c | Inorg. Chem. 2012, 51, 11106−11116

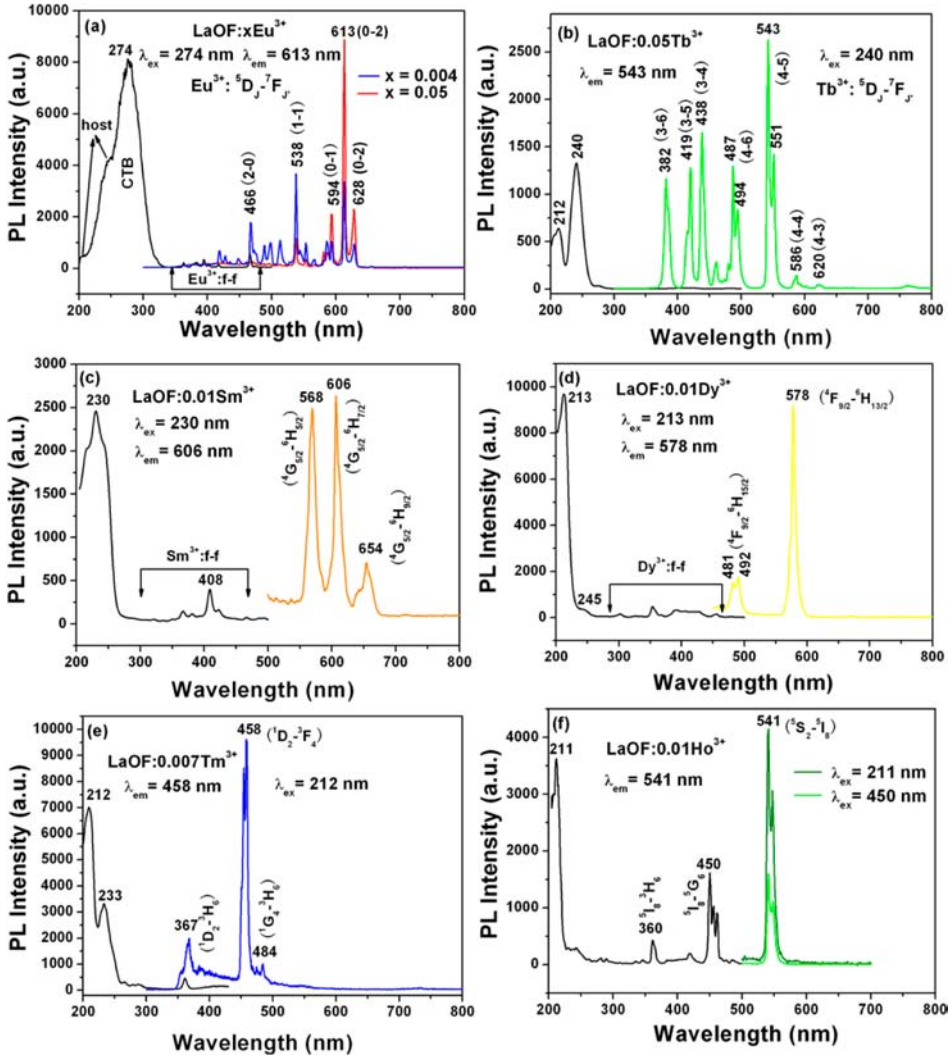

Figure 4. Representative photoluminescence excitation and emission spectra of (a) LaOF:xEu^{3+} (x = 0.004, 0.05), (b) LaOF:0.05Tb^{3+}, (c) LaOF:0.01Sm^{3+}, (d) LaOF:0.01Dy^{3+}, (e) LaOF:0.007Tm^{3+}, and (f) LaOF:0.01Ho^{3+}.

i.e., $^5D_3 \rightarrow {}^7F_1$ (419 nm), $^5D_3 \rightarrow {}^7F_2$ (428 nm), $^5D_3 \rightarrow {}^7F_3$ (447 nm), $^5D_2 \rightarrow {}^7F_0$ (467 nm), $^5D_2 \rightarrow {}^7F_2$ (488 nm), $^5D_2 \rightarrow {}^7F_3$ (513 nm), $^5D_1 \rightarrow {}^7F_1$ (538 nm), $^5D_1 \rightarrow {}^7F_2$ (553 nm), $^5D_1 \rightarrow {}^7F_3$ (586 nm), $^5D_0 \rightarrow {}^7F_1$ (593 nm), $^5D_0 \rightarrow {}^7F_2$ (613 nm), $^5D_0 \rightarrow {}^7F_3$ (650 nm).[23,24] The strongest one is located at 538 nm ($^5D_1 \rightarrow {}^7F_1$). With increasing Eu^{3+} doping concentration, the higher-level $^5D_{1,2,3}$ emissions are quenched gradually, and the lower energy level ($^5D_0$) emission becomes dominating, which can be observed from the emission spectrum of the LaOF:0.05Eu^{3+} sample (red line). The CIE coordinates for the LaOF:xEu^{3+} (x = 0.004, 0.05) samples are shown in points 1 and 2 in Figure 5, respectively. So the luminescence color of the LaOF:Eu^{3+} samples can be tuned by adjusting the doping concentration of Eu^{3+} ion, which is consistent with the previous report.[21] Furthermore, the dependence of PL intensity (Eu^{3+}: $^5D_1 \rightarrow {}^7F_1$ and $^5D_0 \rightarrow {}^7F_2$) on Eu^{3+} ions doping concentration in the LaOF:xEu^{3+} samples is shown in Figure S3 (Supporting Information). The intensity of the emission from $^5D_1 \rightarrow {}^7F_1$ increases with increasing Eu^{3+} ion concentration and gradually decreases as the doping concentration becomes higher than x = 0.008. The average distance (R) between Eu^{3+} ions can also be estimated in terms of the equation $R = 2 \times [3V/(4\pi xN)]^{1/3}$ (where V is the volume of the unit cell, x is the concentration, and N is the number of available crystallographic sites occupied by the activator ions in the unit cell).[25] The related crystal parameters V and N for LaOF are 286.47 Å^3 and 6, respectively. The corresponding calculated R (Eu^{3+}−Eu^{3+}) value for LaOF:0.008Eu^{3+} is determined to be 20.90 Å. As the Eu^{3+} doping concentration increases, the Eu^{3+}−Eu^{3+} distance becomes small enough (shorter than 20.90 Å) to allow a resonant energy transfer, and the higher energy level $^5D_1$ is quenched by the cross relaxation process: Eu^{3+} ($^5D_1$) + Eu^{3+} ($^7F_0$) → Eu^{3+} ($^5D_0$) + Eu^{3+} ($^7F_3$).[26] However, the emission intensity of Eu^{3+} ($^5D_0 \rightarrow {}^7F_2$) reaches a maximum value at x = 0.05 and then decreases with further increasing its concentration. Different from the cross-relaxation quenched mechanism of Eu^{3+} ($^5D_1 \rightarrow {}^7F_1$), the concentration quenching of Eu^{3+} ($^5D_0 \rightarrow {}^7F_2$) is caused by energy transfer between luminescent centers. In the energy migration process, the excitation energy will be lost at a killer or quenching site.[26]

Similar to the luminescence property of Eu^{3+} ion in the LaOF host, the luminescence color of Tb^{3+} ion also depends on its doping concentration. Generally, with a low doping concentration of Tb^{3+} in host matrix, the transitions of $^5D_3$ to ^7F_J dominate and produce the blue emissions. As Tb^{3+} concentration increases, the cross relaxation from $^5D_3$ to $^5D_4$

dx.doi.org/10.1021/ic301662c | Inorg. Chem. 2012, 51, 11106−11116

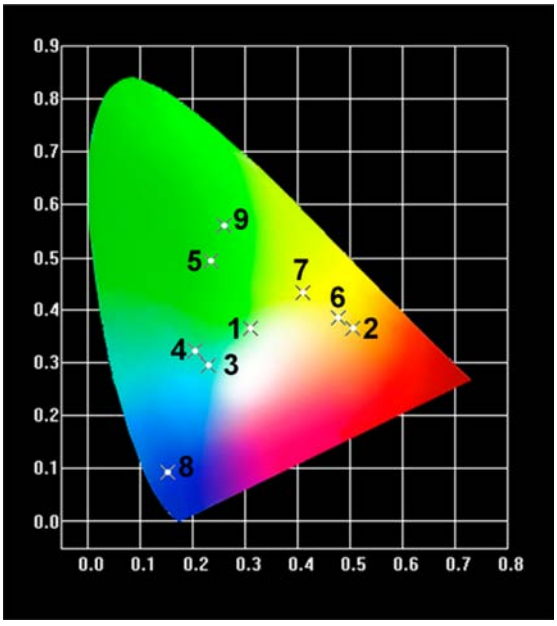

Figure 5. The CIE chromaticity diagram for (1) LaOF:0.004Eu^{3+}, (2) LaOF:0.05Eu^{3+}, (3) LaOF:0.005Tb^{3+}, (4) LaOF:0.01Tb^{3+}, (5) LaOF:0.10Tb^{3+}, (6) LaOF:0.01Sm^{3+}, (7) LaOF:0.01Dy^{3+}, (8) LaOF:0.007Tm^{3+}, and (9) LaOF:0.01Ho^{3+}.

occurs (Tb^{3+}: $^5D_3 + {}^7F_6 \rightarrow {}^5D_4 + {}^7F_{0,1}$) owing to the interaction between Tb^{3+} ions, which enhances the transitions of $^5D_4$ to ^7F_J with a green emission,[26] which can be confirmed by the CIE coordinates for the LaOF:Tb^{3+} samples with different doping concentrations. The points 3, 4, 5 in Figure 5 show the CIE coordinates of the LaOF:0.005Tb^{3+}, LaOF:0.01Tb^{3+}, and LaOF:0.10Tb^{3+} samples, respectively. It can be observed that the luminescence color can be tuned from blue to green. Figure 4b shows the representative PL excitation and emission spectra of the LaOF:0.05Tb^{3+} sample. The excitation spectrum consists of two brand bands from 200 to 300 nm with maximum at 212 and 240 nm, respectively, which are attributed to the $4f^8 \rightarrow 4f^7 5d$ transition absorption of Tb^{3+} ions. Under 240 nm UV excitation, the emission spectrum of the LaOF:0.05Tb^{3+} sample consists of the $^5D_{3,4} \rightarrow {}^7F_J$ transitions of Tb^{3+}, i.e., 382 nm (3−6), 419 nm (3−5), 438 nm (3−4), 487 nm (4−6), 543 nm (4−5), 586 nm (4−4), 620 nm (4−3), respectively.[26] The photoluminescence intensity of Tb^{3+} ($^5D_3 \rightarrow {}^7F_4$) and Tb^{3+} ($^5D_4 \rightarrow {}^7F_5$) as a function of its content (y) in LaOF:$y$$Tb^{3+}$ is also shown in Figure S3 (Supporting Information). The concentration quenching mechanism for Tb^{3+} is similar to Eu^{3+} ion.

For the LaOF:Sm^{3+} samples, they give the emissions at 568, 606, and 654 nm under 230 nm UV excitation (Figure 4c), which correspond to the transitions from $^4G_{5/2}$ to $^6H_{5/2}$, $^6H_{7/2}$, $^6H_{9/2}$ of Sm^{3+}, respectively.[26,27] The corresponding CIE coordinates are located in the yellow-orange zone, as shown in point 6 in Figure 5. Moreover, the excitation band from 200 to 300 nm in the excitation spectrum of the LaOF:0.01Sm^{3+} sample comes from the CTB between Sm^{3+} and O^{2-}. Since the transition of $^4G_{5/2} \rightarrow {}^6F_{9/2}$ and $^6H_{5/2} \rightarrow {}^6F_{9/2}$ of Sm^{3+} ion require approximately equal energy, the concentration quenching of Sm^{3+} ions easily happens due to the cross-relaxation effect: Sm^{3+} ($^4G_{5/2}$) + Sm^{3+} ($^6H_{5/2}$) → $2Sm^{3+}$ ($^6F_{9/2}$). So the optimum concentration of Sm^{3+} in the LaOF host is relatively low, as shown in Figure S3 (Supporting Information).

Figure 4d presents the PL excitation and emission spectra of the LaOF:0.01Dy^{3+} sample. Monitored with the characteristic $^4F_{9/2} \rightarrow {}^6H_{13/2}$ emission of Dy^{3+} at 578 nm, the excitation spectrum shows two absorption bands with peak at 213 nm (intense) and 245 nm (weak) and some line absorptions from the f-f transitions of Dy^{3+} ion. According to the PL excitation spectrum of the LaOF:Eu^{3+} sample, the two excitation bands come from the host absorption. Upon excitation with 213 nm irradiation, the emission spectrum of Dy^{3+} is dominated by two main groups of emission in the blue region with a maximum at 492 nm and the yellow region with a maximum at 578 nm. These emissions correspond to the transitions from $^4F_{9/2}$ to $^6H_{15/2}$ and $^6H_{13/2}$ of Dy^{3+}, respectively.[26] This indicates that the LaOF host can transfer its energy to Dy^{3+} ions. The similar situation will hold for the LaOF:Tm^{3+}/Ho^{3+} samples. In addition, the concentration quenching of Dy^{3+} is also owing to the cross-relaxation effect (Dy^{3+}: $^4F_{9/2} + {}^6H_{15/2} \rightarrow {}^6F_{2/3} + {}^6F_{11/2}$) like Sm^{3+} ion and the relation curve of Dy^{3+} concentration, and its PL intensity is shown in Figure S3 (Supporting Information).

Tm^{3+} ion is always used as efficient blue light emissive activator and the blue emissions mainly result from $^1D_2 \rightarrow {}^3H_6$, $^1D_2 \rightarrow {}^3F_4$, and $^1G_4 \rightarrow {}^3H_6$ transitions of Tm^{3+} ion. The PL spectra of the LaOF:0.007Tm^{3+} sample are shown in Figure 4e. The excitation spectrum shows the host excitation from 200 to 250 nm and a sharp peak at 360 nm assigned to the $^3H_6 \rightarrow {}^1D_2$ transition of Tm^{3+}. Under the host excitation at 212 nm, the emission spectrum consists of $^1D_2 \rightarrow {}^3H_6$ (367 nm), $^1D_2 \rightarrow {}^3F_4$ (458 nm), and $^1G_4 \rightarrow {}^3H_6$ (484 nm) of Tm^{3+}, and the CIE coordinates locate at the blue region with higher color purity, as shown in point 8 in Figure 5. Figure S3 (Supporting Information) shows the PL intensity as a function of Tm^{3+} doping concentration. It can be observed that the optimum doping concentration of Tm^{3+} in LaOF host is 0.3 mol % of La^{3+}. Different from Sm^{3+} and Dy^{3+} ions, there are no matched energy levels to quench the emissions from $^1D_2$ level of Tm^{3+}, so the quenching is not due to cross relaxation but because of the energy migration among the activator ions, which is similar to the $^5D_0$ level of Eu^{3+} ion. It is well-known that blue and yellow light mixed in suitable proportions will show a white light.[28−31] So in our current study, we tried to obtain white emission by codoping Tm^{3+} and Dy^{3+} as well as the elaborate choice of doping levels in the LaOF single host. Our experimental results further confirm the above fact, and this part will be investigated in the following cathodoluminescence properties in detail.

Figure 4f shows the PL spectra of the LaOF:0.01Ho^{3+} sample. Similar to Tm^{3+} and Dy^{3+} ions, its excitation spectrum contains the absorption of host and the f-f transition of Ho^{3+}. However, the absorption peak at 450 nm coming from the $^5I_8 \rightarrow {}^5G_6$ transition of Ho^{3+} has a relatively high intensity compared with other Ln^{3+} (Ln = Eu, Tb, Dy, Sm, or Tm) ions in the LaOF host. Upon excitation with 211 nm (host) and 450 nm (the $^5I_8 \rightarrow {}^5G_6$ transition of Ho^{3+}) irradiation, the emission spectra present one dominated peak at 541 nm due to the $^5S_2 \rightarrow {}^5I_8$ transition of Ho^{3+} and so give a green emission as shown in point 9 in Figure 5.

It has been recognized that the luminescence intensities of various rare earth ions can be enhanced or quenched by the energy transfer from other codoped rare ions.[32] For example, an energy transfer can take place from Tb^{3+} to Eu^{3+} when they are codoped in one host, and the energy transfer properties

dx.doi.org/10.1021/ic301662c | Inorg. Chem. 2012, 51, 11106−11116

from Tb^{3+} to Eu^{3+} have been investigated in detail.[23,33] However, only limited information is available on the energy transfer from Tm^{3+} to Ho^{3+}. In our experiment, as shown in Figure 6a, there is an overlap between the PL emission

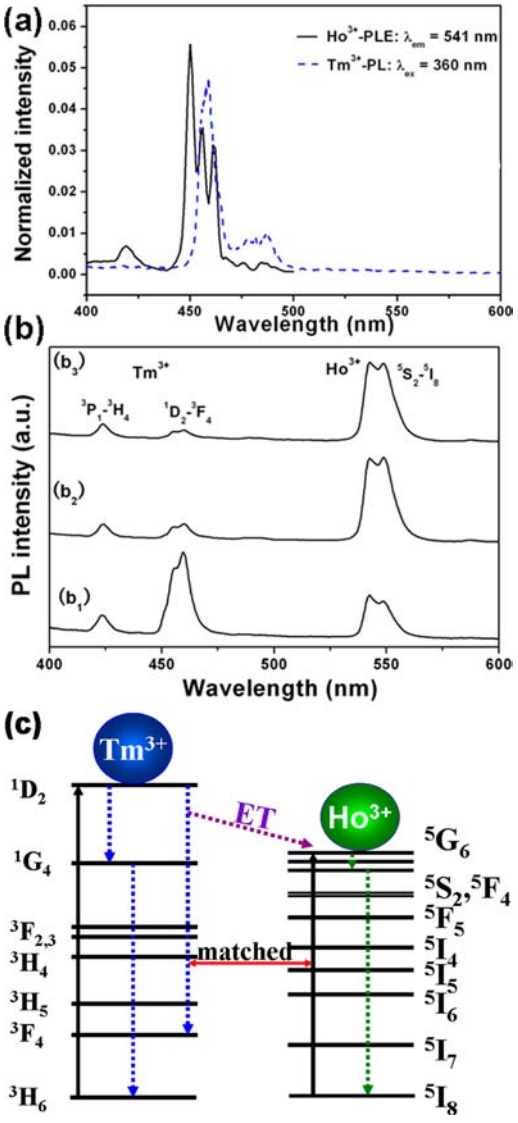

Figure 6. (a) Spectra overlap between the photoluminescence emission (PL) spectrum of LaOF:Tm^{3+} (blue dash line) and the photoluminescence excitation (PLE) spectrum of LaOF:Ho^{3+} (black solid line). (b) The PL spectra of the LaOF:0.003Tm^{3+}, $k$$Ho^{3+}$ samples with different Ho^{3+} concentration: (b_1) k = 0.001, (b_2) k = 0.005, and (b_3) k = 0.007 under the excitation of 360 nm. (c) The schematic diagram of the relevant Tm^{3+} and Ho^{3+} energy levels and transitions in a down-conversion process.

spectrum of Tm^{3+} and the excitation spectrum of Ho^{3+}, so we can deduce that Tm^{3+} can transfer its energy to Ho^{3+} when they are codoped in the LaOF host. Herein, we investigated the energy transfer properties from Tm^{3+} to Ho^{3+} in the γ-phase LaOF host for the first time. Figure 6b shows the PL spectra of the LaOF:0.003Tm^{3+}, $k$$Ho^{3+}$ (k = 0.001, 0.005, and 0.007) samples with different Ho^{3+} concentration under the excitation of the $^3H_6 \rightarrow {}^1D_2$ transition of Tm^{3+} at 360 nm. It can be observed that the green emission band at 541 nm and a weak blue emission band at 458 nm are obtained in the LaOF:0.003Tm^{3+}, $k$$Ho^{3+}$ samples while pumping the $^3H_6 \rightarrow {}^1D_2$ transition of Tm^{3+} at 360 nm. Moreover, the blue emission of Tm^{3+} decreases with the increase of Ho^{3+} doping concentration, while the green emission of Ho^{3+} increases. The appearance of Ho^{3+}: $^5S_2 \rightarrow {}^5I_8$ strong fluorescence suggests that the energy transfer occurs from Tm^{3+} to Ho^{3+}. The possible energy transfer mechanism is shown in Figure 6c. The energy difference between $^1D_2$ and $^3F_4$ of Tm^{3+} matches well with that between $^5I_8$ and $^5G_6$ of Ho^{3+}, which makes the energy transfer from Tm^{3+} to Ho^{3+} efficient. In addition, the critical distance R_{Tm-Ho} of energy transfer from the Tm^{3+} to Ho^{3+} can be calculated using the concentration quenching method: $R_{Tm-Ho} = 2 \times [3\ V/(4\pi x_c N)]^{1/3}$ (where V is the volume of the unit cell, x is the total concentration of Tm^{3+} and Ho^{3+}, and N is the number of available crystallographic sites occupied by the activator ions in the unit cell).[25] As mentioned earlier, for the LaOF host, V = 286.47 Å^3 and N = 6. The critical concentration x_c, at which the luminescence intensity of Tm^{3+} is half of that in the absence of Ho^{3+}, is 0.4%. Therefore, the critical distance (R_{Tm-Ho}) of energy transfer was calculated to be about 28.4 Å. This value is much longer than the 4 Å, indicating little possibility of energy transfer via the exchange interaction mechanism. Thus, the energy transfer between the Tm^{3+} and Ho^{3+} ions mainly takes place by multipolar interactions. According to the Dexter's energy-transfer expressions of multipolar interaction and Reisfeld's approximation, the following relation can be given[25,34,35]

$$\frac{I_{S0}}{I_S} \propto C_{Tm+Ho}^{n/3}$$

where I_{S0} is the intrinsic luminescence intensity of Tm^{3+}, I_S is the luminescence intensity of Tm^{3+} in the presence of the Ho^{3+}, and n = 6, 8, 10 correspond to dipole−dipole, dipole−quadrupole, and quadrupole−quadrupole interactions, respectively. The I_{S0}/I_S-$C_{Tm+Ho}^{n/3}$ plots are shown in Figure S4 (Supporting Information), and the relationships are observed when n = 6, 8, 10. The plot for n = 10 has the best linear fitting result, which indicates that the energy transfer mechanism from Tm^{3+} to Ho^{3+} is a quadrupole−quadrupole interaction type. In order to further validate the energy transfer from Tm^{3+} to Ho^{3+}, we also investigated the decay curves of Tm^{3+}. The decay behavior of Tm^{3+} can be expressed as $I = I_0 \exp(-t/\tau)$,[26] where I and I_0 are the luminescence intensities at time t and 0, and τ is the luminescence lifetime. Figure S5A (Supporting Information) shows the representative decay curves of Tm^{3+} emission in the LaOF:0.005 Tm^{3+} and LaOF:0.005 Tm^{3+}, 0.003Ho^{3+} samples excited at 360 nm and monitored at 458 nm. For the LaOF:0.005 Tm^{3+}, $k$$Ho^{3+}$ (k = 0, 0.001, 0.003, 0.005, 0.007, 0.009) samples, the lifetime of Tm^{3+} decreases with increasing Ho^{3+} concentration, which are 7.2, 5.41, 5.1, 3.66, 2.59, and 0.89 μs, respectively. The τ_{S0}/τ_S-$C_{Tm+Ho}^{n/3}$ plots are shown in Figure S5B (Supporting Information), and the relationships for n = 10 have the best linear fitting result, which is consistent with the result obtained by calculating photoluminescence intensity of Tm^{3+}. Therefore, the electric quadrupole−quadrupole interaction predominates in the energy transfer process betwen Tm^{3+} and Ho^{3+} ions in the LaOF host. The same situation holds for LaOF:Tb^{3+}, Eu^{3+}(Sm^{3+}) and LaOF:Tm^{3+}, Eu^{3+} codoped systems that will not be discussed here. Furthermore, the energy transfer among activator ions (Tb^{3+}, Tm^{3+}, Sm^{3+}, Eu^{3+}, Ho^{3+}) privies an approach to tune emission colors. On the other hand, the simultaneous luminescence of Eu^{3+}, Tb^{3+}, Sm^{3+}, Dy^{3+}, Tm^{3+}, or Ho^{3+} in the LaOF host is the

dx.doi.org/10.1021/ic301662c | Inorg. Chem. 2012, 51, 11106−11116

other approach to tune the emission colors in the studied compounds. Although there is strong interaction including quenching luminescence between the activators and each other, the simultaneous luminescence of Tb^{3+}, Tm^{3+}, Eu^{3+}, Sm^{3+}, Dy^{3+} or Ho^{3+} individually plays an important role in tuning luminescent colors. Moreover, the Tb^{3+} and Tm^{3+} ions are not good energy transfer donors to Eu^{3+} and Sm^{3+} ions in the LaOF host. Therefore, the multicolors in Figure 10 mainly originate the simultaneously of Tb^{3+}, Tm^{3+}, Eu^{3+}, Sm^{3+}, Dy^{3+}, or Ho^{3+} individually, rather than through energy transfer. The color-tunable luminescence will be investigated by change the doping concentrations of activator ions (Tb^{3+}, Tm^{3+}, Eu^{3+}, Sm^{3+}, Dy^{3+} , or Ho^{3+}) in detail in the CL section.

3.3. Cathodoluminescence Properties. $LaCO_3F:Ln^{3+}$ (Ln = Eu, Tb, Sm, Dy, Tm, and/or Ho) precursors are unstable under electron beam excitation and easily decomposed, so their cathodoluminescence properties cannot be measured. However, the $LaOF:Ln^{3+}$ samples exhibit excellent luminescence properties under low-voltage electron beam excitation. For the $LaOF:Eu^{3+}$, $LaOF:Sm^{3+}$, $LaOF:Dy^{3+}$, $LaOF:Tm^{3+}$, $LaOF:Ho^{3+}$ samples, the CL spectral profiles are similar to their PL spectra. The CL spectra and the luminescence photographs of the $LaOF:Sm^{3+}$, $LaOF:Dy^{3+}$, $LaOF:Tm^{3+}$, and $LaOF:Ho^{3+}$ samples are shown in Figure 7.

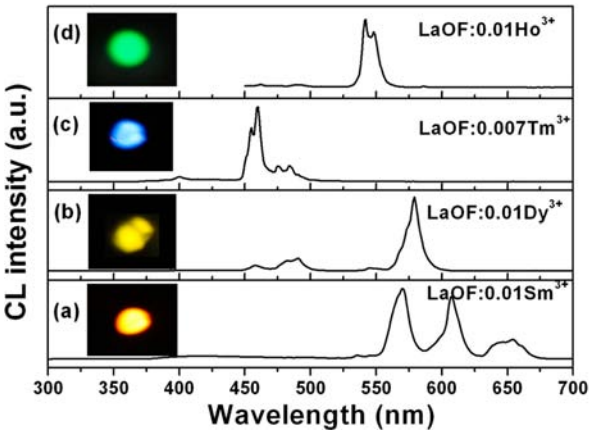

Figure 7. Typical CL spectra of (a) $LaOF:0.01Sm^{3+}$, (b) $LaOF:0.01Dy^{3+}$, (c) $LaOF:0.007Tm^{3+}$, and (d) $LaOF:0.01Ho^{3+}$ under low-voltage electron beam (accelerating voltage = 4 kV, filament current = 94 mA).

Under low-voltage electron beam excitation, the $LaOF:Sm^{3+}$, $LaOF:Dy^{3+}$, $LaOF:Tm^{3+}$, and $LaOF:Ho^{3+}$ samples give a bright yellowish-orange, yellow, blue, and green emission due to the characteristic transitions of Sm^{3+}, Dy^{3+}, Tm^{3+}, and Ho^{3+}, respectively. For $LaOF:Eu^{3+}$ nanocrystals, they can emit tunable color by adjusting Eu^{3+} doping concentration under the low-voltage excitation, similar with their PL properties.[21] However, the CL spectra of the $LaOF:Tb^{3+}$ samples are quite different from their PL spectra. Figure 8 shows the difference between CL and PL spectra of the $LaOF:0.005Tb^{3+}$ sample. It is obvious that the relative intensity of the transitions of $^5D_3 \rightarrow {}^7F_{4,5,6}$ compared with the transition of $^5D_4 \rightarrow {}^7F_5$ in the PL spectrum are stronger than that in the CL spectrum. Under the UV light excitation, with a low doping concentration of Tb^{3+} in the LaOF host, the transitions of $^5D_3$ to ^7F_J dominate and produce the blue emission. However, under electron-beam excitation, the $LaOF:Tb^{3+}$ samples only exhibit green emission even if Tb^{3+} ions has a low doping concentration. The difference

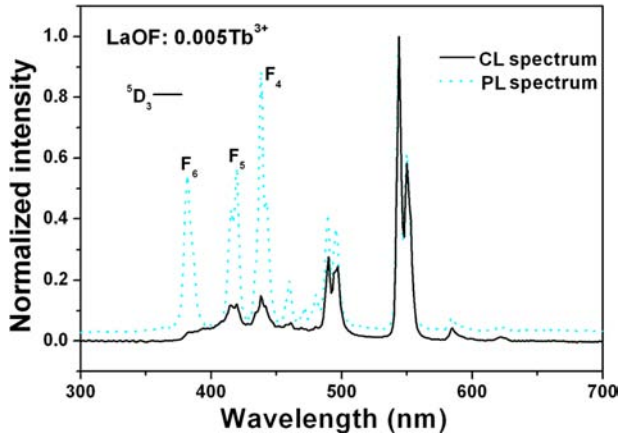

Figure 8. The CL spectrum of the $LaOF:0.005Tb^{3+}$ sample under low-voltage electron beam (accelerating voltage = 4 kV, filament current = 94 mA); its PL spectra (dash line) is shown for comparison.

between the CL and PL spectral profiles can be attributed to their different luminescence mechanisms. The ultraviolet and/or visible light usually excites the activator directly; the fast electrons as high energy particles always excite the host lattice.[26] For CL, the primary fast electrons create many secondary electrons. These secondary electrons excite the host lattice and create many electron−hole pairs, leading to the formation of bound excitons. These excitons decay non-radiatively through a resonant or quasi-resonant transfer to the Tb^{3+}. In the LaOF host, the energy of bound excitons may be lower than the energy of Tb^{3+} $^5D_3$ level, resulting in only green emission under electron-beam excitation. In addition, for a purpose of comparison, the emission spectra of commercial phosphors ZnO:Zn (green) and $Y_2SiO_5:Ce^{3+}$ (blue) are shown in Figure S6 (black line, Supporting Information), which all show broad band emissions with maxima at 497 and 420 nm, respectively. The CIE coordinates of ZnO:Zn and $Y_2SiO_5:Ce^{3+}$ are determined to be (0.2053, 0.3879) and (0.1651, 0.1568), respectively. For CL, the efficiency of a luminescent material includes the radiant efficiency (η) and the luminous efficiency (L, brightness),[26] which can be compared roughly by their emission peak areas (integrated luminescence intensity) and the CL intensity (in height), respectively. The comparison for η and L between commercial phosphors (ZnO:Zn and $Y_2SiO_5:Ce^{3+}$) and as-prepared samples is shown in Figure 9a and b, which is calculated from Figure S6 (Supporting Information). It can be seen that under the same excitation condition, the emission peak areas (Figure 9a) of the $LaOF:0.07Tb^{3+}$, $LaOF:0.07Ho^{3+}$, and $LaOF:0.005Tm^{3+}$ are smaller than that of ZnO:Zn and $Y_2SiO_5:Ce^{3+}$; however, the CL intensity (Figure 9b) of the $LaOF:0.07Tb^{3+}$ is higher than that of the ZnO:Zn, and the $LaOF:0.005Tm^{3+}$ sample has the comparative CL intensity with the $Y_2SiO_5:Ce^{3+}$ blue phosphor. Moreover, the CIE coordinates (emission color) of $LaOF:0.07Tb^{3+}$ (0.2521, 0.5647) and $LaOF:0.005Tm^{3+}$ (0.1510, 0.0761) are more saturated than those of ZnO:Zn and $Y_2SiO_5:Ce^{3+}$ respectively, as shown in Figure 9c. The CL photographs labeled as 1, 2, 3, and 4 represent the luminescence colors of $LaOF:0.07Tb^{3+}$, ZnO:Zn, $LaOF:0.005Tm^{3+}$, and $Y_2SiO_5:Ce^{3+}$, respectively. It can be obviously seen that the color purity of $LaOF:0.07Tb^{3+}$ and $LaOF:0.005Tm^{3+}$ is higher than that of ZnO:Zn and

dx.doi.org/10.1021/ic301662c | Inorg. Chem. 2012, 51, 11106−11116

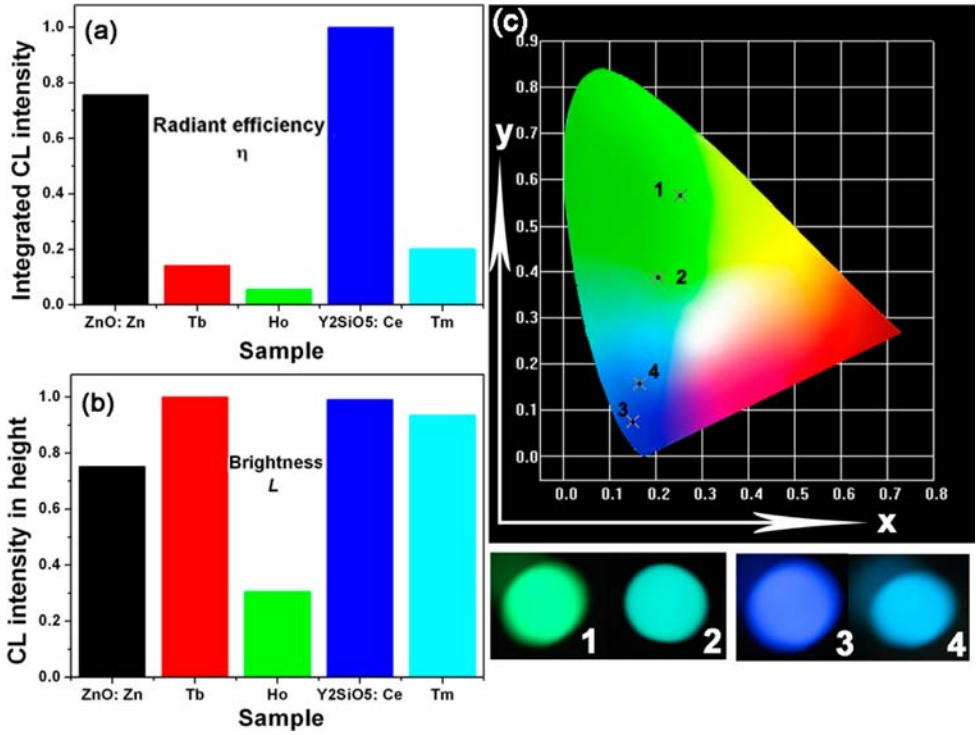

Figure 9. (a, b) The diagram for η (radiation efficiency) and L (brightness) of the commercial phosphors (ZnO:Zn and $Y_2SiO_5:Ce^{3+}$) and as-prepared samples ($LaOF:0.07Tb^{3+}/0.07Ho^{3+}/0.005Tm^{3+}$). (c) The CIE chromaticity diagram for $LaOF:0.07Tb^{3+}$ (1), ZnO:Zn (2), $LaOF:0.005Tm^{3+}$ (3), and $Y_2SiO_5:Ce^{3+}$ (4). The digital photographs represent their respective catodoluminescence color.

$Y_2SiO_5:Ce^{3+}$ phosphors, which is more advantageous to full color field emission display.

It is well-known that the multicolored emission can be realized by mixing the tricolor (red, green, and blue) composition at a proper ratio.[36] Because the simultaneous luminescence of Eu^{3+}, Tb^{3+}, Sm^{3+}, Dy^{3+}, Tm^{3+}, and Ho^{3+} can occur in the LaOF host, it is possible to simultaneously present their characteristic emissions in the co- or tridoped systems, such as the $LaOF:Tm^{3+}$, Dy^{3+}, $LaOF:Tb^{3+}$, Sm^{3+}, and $LaOF:Tm^{3+}$, Ho^{3+}, Eu^{3+} systems. Then various luminescence colors can be realized by adjusting the relative doping concentrations of the dopant ions, as depicted by Figure S7 (Supporting Information). Figure 10 shows typical CL spectra of the $LaOF:0.07Tb^{3+}$, $0.05Eu^{3+}$, $LaOF:0.01Tb^{3+}$, $0.007Sm^{3+}$, $LaOF:0.003Tm^{3+}$, $0.005Dy^{3+}$, $LaOF:0.005Tm^{3+}$, $001Ho^{3+}$, $0.11Eu^{3+}$, and $LaOF:0.003Tm^{3+}$, $0003Ho^{3+}$ samples and their corresponding CL digital photographs. Obviously, it can be seen that in the codoping or tridoping systems, the emissions of dopant ions simultaneously appear with different luminescence intensities. Therefore, the CL colors can be tuned from green to orange then to red or from blue to cyan to white to yellow by varying the dopant ions and their doping concentration, as shown in Figure 10. The CL spectra and the CIE coordinates of the $LaOF:Ln^{3+}$ samples with other Ln^{3+} doping concentration under low-voltage electron beam (accelerating voltage = 4 kV, filament current = 94 mA) are shown in Figure S8 (Supporting Information). These abundant luminescence colors and wide color region of the $LaOF:Ln^{3+}$ (Ln = Eu, Tb, Sm, Dy, Ho, and/or Tm) phosphors under low-voltage electron beam excitation contribute great potential application in field emission displays.

The normalized CL emission intensities of $LaOF:0.003Tm^{3+}$, $0.01Ho^{3+}$, $0.05Eu^{3+}$, $LaOF:0.003Tm^{3+}$, $0.01Dy^{3+}$, $LaOF:0.01Dy^{3+}$, and $LaOF:0.01Sm^{3+}$ have been investigated

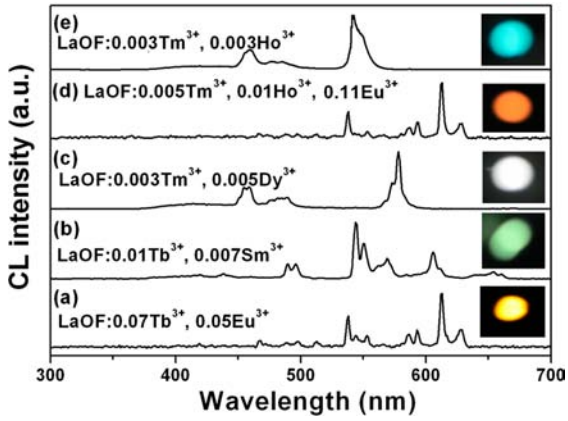

Figure 10. Typical CL spectra of the $LaOF:RE^{3+}$ samples: (a) $LaOF:0.07Tb^{3+}$, $0.05Eu^{3+}$, (b) $LaOF:0.01Tb^{3+}$, $0.007Sm^{3+}$, (c) $LaOF:0.003Tm^{3+}$, $0.005Dy^{3+}$, (d) $LaOF:0.005Tm^{3+}$, $001Ho^{3+}$, $0.11Eu^{3+}$, and (e) $LaOF:0.003Tm^{3+}$, $0003Ho^{3+}$ (accelerating voltage = 4 kV, filament current = 94 mA). The insets are their corresponding CL digital photographs.

as a function of the accelerating voltage and the filament current, as shown in Figure 11. It is worth noting that the *y*-axis of Figure 11 is presented in the format of "normalized intensity", and so the intensity does not represent the luminescence intensity. The intensities of different samples with the same conditions have no comparability. When the filament current is fixed at 92 mA, the CL intensity increases with raising the accelerating voltage from 2.0 to 7.0 kV (Figure 11a). Similarly, under a 4.5 kV electron beam excitation, the CL intensity also increases with increasing the filament current from 82 to 94 mA (Figure 11b). There is no obvious saturation effect for the CL intensity of these samples with the increase of

dx.doi.org/10.1021/ic301662c | *Inorg. Chem.* 2012, 51, 11106−11116

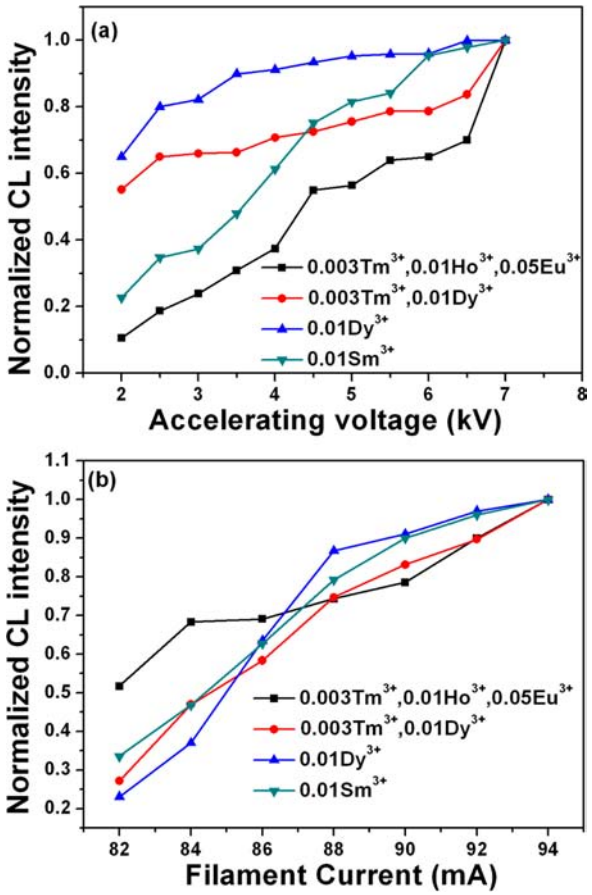

Figure 11. The cathodoluminescence intensity of the LaOF:0.01Sm^{3+}, LaOF:0.01Dy^{3+}, LaOF:0.003Tm^{3+}, 0.01Dy^{3+}, and LaOF:0.005Tm^{3+}, 001Ho^{3+}, 0.05Eu^{3+} samples as a function of the accelerating voltage (a) and the filament current (b).

current density and accelerating voltage. The increase in CL brightness with an increase in electron energy and filament current is attributed to the deeper penetration of the electrons into the phosphor body and the larger electron-beam current density. The electron penetration depth can be estimated using the empirical formula $L[Å] = 250\ (A/\rho)(E/Z^{1/2})^n$, where $n = 1.2/(1-0.29 \log Z)$, A is the atomic or molecular weight of the material, ρ is the bulk density, Z is the atomic number or the number of electrons per molecule in the case of compounds, and E is the energy of the accelerating electron (keV).[37] The higher accelerating voltage and filament current, the larger the energy of the accelerating electron and so the deeper penetration depth. For CL of the above samples, the Tm^{3+}, Tb^{3+}, Dy^{3+} and Ho^{3+}, Eu^{3+}, Sm^{3+} ions are excited by the plasma produced by the incident electrons. The deeper the electron penetration depth, the more plasma will be produced, which results in more activator ions being excited, and thus the CL intensity increases.

The degradation property for phosphor is very important for FED application. Thus we also investigated the degradation behavior of the as-prepared samples under low-voltage electron beam excitation. Figure S9 (Supporting Information) shows the decay behavior of the CL intensity of the representative LaOF:0.07Tb^{3+}, LaOF:0.007Ho^{3+}, and LaOF:0.005Tm^{3+} samples under continuous electron beam bombardment when the accelerating voltage = 2.0 kV, filament current = 88 mA. The CL intensity of the studied samples monotonously decreases with prolonging the electron bombardment time. After the continuous electron radiation for 60 min, the CL intensities of the samples fall to about 75% of the initial value. This degradation of CL intensity may be due to the accumulation of carbon at the surface during electron bombardment, which mainly comes from the carbon nanotube cathode of the excitation source.[38,39] The accretion of graphitic carbon during electron-beam exposure at high current densities is a well-known effect. This carbon contamination will prevent low-energy electrons from reaching the phosphor grains and also exacerbate surface charging, and thus lower the CL intensity. In addition, after stopping bombardment for a while, the CL intensity could not restore to the initial value, indicating permanent damage to the phosphor occurs, which is another reason resulting in the decrease of the CL intensity. On the other hand, the CL peaks are the same as those before electron bombardment. So, the CIE chromaticity coordinates of the LaOF:0.07Tb^{3+} sample under a continuous electron beam radiation are measured to investigate the color stability. After a continuous electron radiation for 1 h, the CIE values are nearly invariable x and y keeps at about 0.2521 and 0.5647, respectively. In summary, the short time experiment (1 h) indicates that the stability of the CL intensity and CIE color coordinates of the as-prepared LaOF:0.07Tb^{3+} sample is good, which shows that LaOF as a host material has potential advantages applied in the FED.

4. CONCLUSIONS

By the hydrothermal method in conjunction with heat-treatment process, LaOF:Ln^{3+} (Ln = Eu, Tb, Sm, Dy, Tm, and/or Ho) nanocrystals with well dispersion have been successfully prepared. Under UV light and low-voltage electron beam excitation, LaOF:Ln^{3+} nanocrystals show the characteristic f-f transitions of Ln^{3+} (Ln = Eu, Tb, Sm, Dy, Tm, or Ho) and give red, blue-green, orange, yellow, blue, and green emission, respectively. More importantly, there exists an energy transfer from Tm^{3+} to Ho^{3+} in the LaOF:Tm^{3+}, Ho^{3+} samples under UV excitation. The energy transfer from Tm^{3+} to Ho^{3+} in LaOF:Tm^{3+}, Ho^{3+} samples has been demonstrated to be a resonant type via a quadrupole−quadrupole mechanism, and the critical distance (R_{Tm-Ho}) calculated by quenching concentration method is 28.4 Å. Under low-voltage electron beam excitation, the LaOF:Tb^{3+} and LaOF:Tm^{3+} phosphors exhibit green and blue luminescence with better chromaticity coordinates, color purity, and higher intensity compared with the commercial green phosphor ZnO:Zn and blue phosphor Y_2SiO_5:Ce^{3+} to some extent. In addition, multicolored luminescence containing white emission have been successfully confected for mono/co/tridoped LaOF:Ln^{3+} (Eu^{3+}, Tb^{3+}, Sm^{3+}, Dy^{3+}, Tm^{3+}, and/or Ho^{3+}) phosphors by adjusting the doping concentrations of Ln^{3+} ions. After the continuous electron radiation for 1 h, the CL intensity of the LaOF:Tb^{3+} sample remains 75% of the initial value, and its CIE coordinates are nearly invariable. All results indicate that these phosphors have potential applications in field emission display devices.

■ ASSOCIATED CONTENT

Supporting Information

The representative XRD patterns of $LaCO_3F$:Eu^{3+}, $LaCO_3F$:Dy^{3+}, $LaCO_3F$:Tb^{3+}, Sm^{3+}, and $LaCO_3F$:Tm^{3+}, Ho^{3+}, Eu^{3+} precursors (Figure S1); representative photoluminescence excitation and emission spectra of $LaCO_3F$:0.03Eu^{3+}, $LaCO_3F$:0.03Tb^{3+}, $LaCO_3F$:0.01Sm^{3+}, $LaCO_3F$:0.02Dy^{3+}, La-

CO_3F:0.01Tm^{3+}, and $LaCO_3F$:0.01Ho^{3+} (Figure S2); the PL intensity of Eu^{3+} ($^5D_1 \rightarrow {}^7F_1$ and $^5D_0 \rightarrow {}^7F_2$), Tb^{3+} ($^5D_3 \rightarrow {}^7F_4$ and $^5D_4 \rightarrow {}^7F_5$), Sm^{3+} ($^4G_{5/2} \rightarrow {}^6H_{7/2}$), Dy^{3+} ($^4F_{9/2} \rightarrow {}^6H_{13/2}$), Tm^{3+} ($^1D_2 \rightarrow {}^3F_4$), and Ho^{3+} ($^5S_2 \rightarrow {}^5I_8$) as a function of its doping concentration (x) in $La_{1-x}OF$:xLn^{3+} (Ln = Eu^{3+}, Tb^{3+}, Sm^{3+}, Dy^{3+}, Tm^{3+}, or Ho^{3+}) (Figure S3); dependence of I_{S0}/I_S of Tm^{3+} on (a) $C_{Tm+Ho}{}^{6/3}$, (b) $C_{Tm+Ho}{}^{8/3}$, and (c) $C_{Tm+Ho}{}^{10/3}$ (Figure S4); decay curves of Tm^{3+} emission in LaOF:0.005 Tm^{3+} and LaOF:0.005 Tm^{3+}, 0.003Ho^{3+} samples excited at 360 nm and monitored at 458 nm and dependence of τ_{S0}/τ_S of Tm^{3+} on (a) $C_{Tm+Ho}{}^{6/3}$, (b) $C_{Tm+Ho}{}^{8/3}$, and (c) $C_{Tm+Ho}{}^{10/3}$ (Figure S5); the cathodoluminescence spectra of (a) LaOF:0.07Tb^{3+}, LaOF:0.007Ho^{3+}, and ZnO:Zn; (b) LaOF:0.005Tm^{3+} and Y_2SiO_5:Ce^{3+} (Figure S6); the CIE chromaticity diagram for the Eu^{3+}, Tb^{3+}, Sm^{3+}, Dy^{3+}, Tm^{3+}, or Ho^{3+} doped LaOF samples, and the solid-lined triangle and arrow depict the tunable color region (Figure S7); the CL spectra of the LaOF:Ln^{3+} (Ln = 0.003Tm, 0.01Eu; 0.005Tm, 0.10Eu; 0.01/0.07Tb, 0.05/0.10Eu; 0.01Tb, 0.007/0.009/0.01Sm; 0.003Tm, 0.005/0.01/0.02Dy; 0.003/0.005Tm, 0.01Ho, 0.05/0.11Eu) samples under low-voltage electron beam (accelerating voltage = 4 kV, filament current = 94 mA) and their corresponding CIE chromaticity diagram (Figure S8); dependence of relative CL intensity of the representative LaOF:0.07Tb^{3+}, LaOF:0.007Ho^{3+}, and LaOF:0.005Tm^{3+} samples on radiation time under the accelerating voltage = 2.0 kV, filament current = 88 mA electron beam excitation. This material is available free of charge via the Internet at http://pubs.acs.org.

AUTHOR INFORMATION

Corresponding Author

*E-mail: jlin@ciac.jl.cn.

Notes

The authors declare no competing financial interest.

ACKNOWLEDGMENTS

This project is financially supported by National Basic Research Program of China (2010CB327704) and the National Natural Science Foundation of China (NSFC 51172227 and 20921002).

REFERENCES

(1) Chalamala, B.; Wei, Y.; Gnade, B. *IEEE Spectrum* **1998**, *35*, 42–51.

(2) Jüstel, T.; Nikol, H.; Ronda, C. *Angew. Chem., Int. Ed.* **1998**, *37*, 3084–3103.

(3) Psuja, P.; Hreniak, D.; Strek, W. *J. Nanomater.* **2007**, *2007*, 81350.

(4) (a) Smet, P. F.; Moreels, I.; Hens, Z.; Poelman, D. *Materials* **2010**, *3*, 2834–2883. (b) Zhang, Q.-H; Wang, J.; Yeh, C.-W.; Ke, W.-C.; Liu, R.-S.; Tang, J.-K.; Xie, M.-B.; Liang, H.-B.; Su, Q. *Acta Mater.* **2010**, *58*, 6728–6735.

(5) Yi, S.; Bae, J. S.; Moon, B. K.; Jeong, J. H.; Park, J.-C.; Kim, I. W. *Appl. Phys. Lett.* **2002**, *81*, 3344–3346.

(6) (a) Geng, D. L.; Li, G. G.; Shang, M. M.; Peng, C.; Zhang, Y.; Cheng, Z. Y.; Lin, J. *Dalton Trans.* **2012**, *41*, 3078–3086. (b) Gomes, J.; Pires, A. M.; Serra, O. A. *Quim. Nova* **2004**, *27*, 706–708.

(7) Lou, Z.; Hao, J. *Thin Solid Films* **2004**, *450*, 334–340.

(8) Holloway, P. H.; Trottier, T. A.; Abrams, B.; Kondoleon, C.; Jones, S. L.; Sebastian, J. S.; Thomes, W. J.; Swart, H. *J. Vac. Sci. Technol., B: Microelectron. Nanometer Struct.–Process., Meas., Phenom.* **1999**, *17*, 758–764.

(9) Yu, M.; Lin, J.; Zhou, Y. H.; Wang, S. B. *Mater. Lett.* **2002**, *56*, 1007–1013.

(10) Hao, J. H.; Cocivera, M. *Appl. Phys. Lett.* **2002**, *81*, 4154.

(11) Li, H.; Wang, Z.; Xu, S.; Hao, J. *J. Electrochem. Soc.* **2009**, *156*, J112–J116.

(12) Jiang, Y. D.; Zhang, F.-L.; Summers, C. J.; Wang, Z. L. *Appl. Phys. Lett.* **1999**, *74*, 1677–1679.

(13) Yang, S.-H.; Yokoyama, M. *J. Vac. Sci. Technol., A* **2001**, *19*, 2463–2467.

(14) Bohren, C. F.; Huffman, D. R. *Absorption and Scattering of Light by Small Particles*; Wiley: New York, 1983; p 132.

(15) Mataki, H.; Yamaki, S.; Fukui, T. *Jpn. J. Appl. Phys.* **2004**, *43*, 5819–5823.

(16) Roh, H.-S.; Kim, D. H.; Park, I.-J.; Song, H. J.; Hur, S.; Kim, D.-W.; Hong, K. S. *J. Mater. Chem.* **2012**, *22*, 12275–12280.

(17) (a) Du, Y. P.; Zhang, Y. W.; Sun, L. D.; Yan, C. H. *J. Phys. Chem. C* **2008**, *112*, 405–415. (b) Grzyb, T.; Lis, S. *Inorg. Chem.* **2011**, *50*, 8112–8120.

(18) (a) Zhang, X. Y.; Gao, D. L.; Li, L. *J. Appl. Phys.* **2010**, *107*, 123528. (b) Balaji, T.; Buddhudu, S. *Spectrosc. Lett.* **1993**, *26*, 113–127.

(19) Antic-Fidancev, E.; Hölsä, J.; Krupa, J.-C.; Lastusaari, M. *J. Alloys Compd.* **2004**, *380*, 303–309.

(20) Hölsä, J. *Acta Chem. Scand.* **1991**, *45*, 583–587.

(21) Shang, M. M.; Li, G. G.; Kang, X. J.; Yang, D. M.; Geng, D. L.; Peng, C.; Cheng, Z. Y.; Lian, H. Z.; Lin, J. *Dalton Trans.* **2012**, *41*, 5571–5580.

(22) Zhang, Y. W.; Jin, S.; Tian, S. J.; Li, G. B.; Jia, T.; Liao, C. S.; Han, C. H. *Chem. Mater.* **2001**, *13*, 372–378.

(23) (a) Li, G. G.; Hou, Z. Y.; Peng, C.; Wang, W. X.; Cheng, Z. Y.; Li, C. X.; Lian, H. Z.; Lin, J. *Adv. Funct. Mater.* **2010**, *20*, 3446–3456. (b) Dorenbos, P. *J. Alloys Compd.* **2009**, *488*, 568–573.

(24) (a) Liu, X. M.; Lin, C. K.; Lin, J. *Appl. Phys. Lett.* **2007**, *90*, 081904. (b) Liu, L. H.; Xie, R.-J.; Hirosaki, N.; Li, Y. Q.; Takeda, T.; Zhang, C.-N.; Li, J. G.; Sun, X. D. *J. Am. Ceram. Soc.* **2010**, *93*, 4081–4086.

(25) Blasse, G. *Philips Res. Rep.* **1969**, *24*, 131–144.

(26) Blasse, G.; Grabmaier, B. C. *Luminescence Materials*; Springer-Verlag: Berlin, 1994; Chapter 4–5.

(27) Liu, X. M.; Lin, J. *J. Mater. Chem.* **2008**, *18*, 221–228.

(28) Jang, H. S.; Kim, H. Y.; Kim, Y.-S.; Lee, H. M.; Jeon, D. Y. *Opt. Express* **2012**, *20*, 2761–2771.

(29) Yang, W.; Chen, T. *Appl. Phys. Lett.* **2006**, *88*, 101903.

(30) Peng, Y.-Y.; Hsieh, T.-E.; Hsu, C.-H. *Nanotechnology* **2006**, *17*, 174–180.

(31) Lu, W.; Luo, Y. S.; Hao, Z. D.; Zhang, X.; Wang, X. J.; Zhang, J. H. *Mater. Lett.* **2012**, *77*, 45–47.

(32) (a) Macedo, A. G.; Ferreira, R. A. S.; Ananias, D.; Reis, M. S.; Amaral, V. S.; Carlos, L. D.; Rocha, J. *Adv. Funct. Mater.* **2010**, *20*, 624–634. (b) Shang, M. M.; Li, G. G.; Kang, X. J.; Yang, D. M.; Geng, D. L.; Lin, J. *ACS Appl. Mater. Interfaces* **2011**, *3*, 2738–2746. (c) Lee, B. H.; Jeong, H. G.; Sohn, K. S. *J. Electronchem. Soc.* **2010**, *157*, J227–J232. (d) Jia, G. H.; Tanner, P. A. *J. Alloys Compd.* **2009**, *471*, 557–560.

(33) (a) Chen, W.; Sammynaiken, R.; Huang, Y. *J. Appl. Phys.* **2000**, *88*, 1424. (b) Yang, J.; Li, G. G.; Peng, C.; Li, C. X.; Zhang, C. M.; Fan, Y.; Xu, Z. H.; Cheng, Z. Y. *J. Solid State Chem.* **2010**, *183*, 451–457. (c) Ruan, Y.; Xiao, Q. B.; Luo, W. Q.; Li, R. F.; Chen, X. Y. *Nanotechnology* **2011**, *22*, 275701.

(34) (a) Reisfeld, R.; Greenberg, E.; Velapoldi, R.; Barnett, B. *J. Chem. Phys.* **1972**, *56*, 1698–1705. (b) Dexter, D. L.; Schulman, J. A. *J. Chem. Phys.* **1954**, *22*, 1063–1070.

(35) Huang, C. H.; Kuo, T. W.; Chen, T. M. *ACS Appl. Mater. Interfaces* **2010**, *2*, 1395–1399.

(36) (a) Ghys, J. D.; Mauricot, R.; Caillier, B.; Guillot, P.; Beaudette, T.; Jia, G. H.; Tanner, P. A.; Cheng, B. M. *J. Phys. Chem. C* **2010**, *114*, 6681–6689. (b) Li, H. C.; Lin, Y. P.; Chou, P. T.; Cheng, Y. M.; Liu, R. S. *Adv. Funct. Mater.* **2007**, *17*, 520–530. (c) Grzyb, T.; Szczeszak, A.; Rozowska, J.; Legendziewicz, J.; Lis, S. *J. Phys. Chem. C* **2012**, *116*, 3219–3226.

(37) Feldman, C. *Phys. Rev.* **1960**, *117*, 455–459.

(38) Xu, X. G.; Chen, J.; Deng, S. Z.; Xu, N. S.; Lin, J. *J. Vac. Sci. Technol., B: Microelectron. Nanometer Struct.–Process., Meas., Phenom.* **2010**, *28*, 490−494.
(39) Zhang, M. C.; Wang, X. J.; Ding, H.; Li, H. L.; Pan, L. K.; Sun, Z. *Int. J. Appl. Ceram. Technol.* **2011**, *8*, 752−758.